

# A Perspective on interfacial engineering of lithium metal anodes and beyond <sup>EP</sup>

Cite as: Appl. Phys. Lett. **117**, 080504 (2020); <https://doi.org/10.1063/5.0018417>

Submitted: 14 June 2020 . Accepted: 13 August 2020 . Published Online: 27 August 2020

Qizhang Yan <sup>id</sup>, Grace Whang <sup>id</sup>, Ziyang Wei, Shu-Ting Ko <sup>id</sup>, Philippe Sautet <sup>id</sup>, Sarah H. Tolbert <sup>id</sup>, Bruce S. Dunn, and Jian Luo <sup>id</sup>

## COLLECTIONS

<sup>EP</sup> This paper was selected as an Editor's Pick



View Online



Export Citation



CrossMark

## ARTICLES YOU MAY BE INTERESTED IN

[Perspective on the pressure-driven evolution of the lattice and electronic structure in perovskite and double perovskite](#)

Applied Physics Letters **117**, 080502 (2020); <https://doi.org/10.1063/5.0014947>

[Heterogeneous photoresponse of individual grain in all-inorganic perovskite solar cells](#)

Applied Physics Letters **117**, 083902 (2020); <https://doi.org/10.1063/5.0014187>

[Atomistic defects as single-photon emitters in atomically thin MoS<sub>2</sub>](#)

Applied Physics Letters **117**, 070501 (2020); <https://doi.org/10.1063/5.0018557>

Lock-in Amplifiers  
up to 600 MHz



Watch



# A Perspective on interfacial engineering of lithium metal anodes and beyond

Cite as: Appl. Phys. Lett. **117**, 080504 (2020); doi: [10.1063/5.0018417](https://doi.org/10.1063/5.0018417)

Submitted: 14 June 2020 · Accepted: 13 August 2020 ·

Published Online: 27 August 2020



View Online



Export Citation



CrossMark

Qizhang Yan,<sup>1</sup>  Grace Whang,<sup>2</sup>  Ziyang Wei,<sup>3</sup>  Shu-Ting Ko,<sup>4</sup>  Philippe Sautet,<sup>3,5</sup>  Sarah H. Tolbert,<sup>2,3</sup>   
Bruce S. Dunn,<sup>2</sup>  and Jian Luo<sup>1,4,a)</sup> 

## AFFILIATIONS

<sup>1</sup>Department of Nanoengineering, University of California San Diego, La Jolla, California 92093, USA

<sup>2</sup>Department of Materials Science and Engineering, University of California, Los Angeles, California 90095, USA

<sup>3</sup>Department of Chemistry and Biochemistry, University of California, Los Angeles, California 90095, USA

<sup>4</sup>Program of Materials Science and Engineering, University of California San Diego, La Jolla, California 92093, USA

<sup>5</sup>Department of Chemical and Biomolecular Engineering, University of California, Los Angeles, California 90095, USA

<sup>a)</sup> Author to whom correspondence should be addressed: [jluo@alum.mit.edu](mailto:jluo@alum.mit.edu)

## ABSTRACT

This Perspective reviews interfacial engineering of lithium metal anodes. Critical issues and open scientific questions related to coatings on the lithium metal anode are discussed. Essential features for ideal coatings, especially those that can potentially enable lithium plating underneath the coating, are highlighted. While most existing approaches use kinetic control to regulate the coating thickness, here we offer a Perspective on thermodynamically controlled interfacial engineering, focusing on spontaneously formed 2D interfacial phases (also known as “complexions”). This approach has been applied to other battery systems but has yet to be realized for lithium metal anodes.

Published under license by AIP Publishing. <https://doi.org/10.1063/5.0018417>

The development of lithium-ion batteries (LIBs) has played an indispensable role in the advancement of modern-day electronics. From the very beginning, lithium (Li) has been viewed as the ideal choice for the anode, as demonstrated with the Li-TiS<sub>2</sub> battery developed at Exxon in the 1970s.<sup>1</sup> However, the formation of Li dendrites, after repeated plating and stripping, produced safety concerns that directed research toward alternative anode materials. Today, commercially available Li-ion batteries depend on intercalation chemistries where lithium ions are shuttled back and forth between a graphite anode and a layered transition metal oxide cathode such as LiCoO<sub>2</sub>. While traditional “rocking chair” batteries demonstrate an excellent cycle life and stability, next-generation Li-ion batteries must push beyond intercalation chemistries in order to attain higher energy densities. To do this, two factors are critical: (1) specific capacity, which refers to how much charge can be stored per mass, and (2) the working voltage window, which is defined by the potential difference between the cathode and the anode redox pair. With these two primary considerations, Li metal has re-emerged as the anode of choice.

In order to address the issues surrounding the use of Li, it is important to revisit its previous performance. Figure 1(a) shows the main mechanisms for degradation and failure in Li metal anodes. Li

deposition typically exhibits a dendritic morphology that has been shown to penetrate across the cell and reach the cathode, resulting in an internal short and subsequently thermal runaway of the battery.<sup>2–6</sup> In addition, the low reduction potential of lithium makes it inherently unstable in conventional electrolytes, resulting in the reduction of the electrolyte to form a passivation layer on the Li surface, commonly known as the “solid-electrolyte interphase (SEI).”<sup>7</sup> Li<sub>2</sub>O, Li<sub>2</sub>CO<sub>3</sub>, LiF, and Li alkylcarbonate are some of the important components that build up the SEI layer depending on the electrolyte systems.<sup>8,9</sup> Defects and cracks in the SEI can result in localized Li-ion flux and trigger dendrite growth.<sup>10</sup> The formation of Li dendrites increases the surface area of the Li anode, resulting in an irreversible consumption of active Li to form a new SEI. In addition, the dendrites can also be pinched off from the bulk Li, which is another avenue in irreversible loss of active lithium. The consequence of these two coupled behaviors leads to poor Coulombic efficiency. Numerous strategies have been reported to mitigate these issues, as shown in Fig. 1(b), including electrolyte additives for creating a stable SEI,<sup>11,12</sup> 3D lithiophilic host structures for guided Li plating,<sup>13,14</sup> separator engineering for dendrite detection<sup>15,16</sup> or anion regulation,<sup>17,18</sup> and Li-electrolyte interfacial engineering.<sup>19,20</sup>

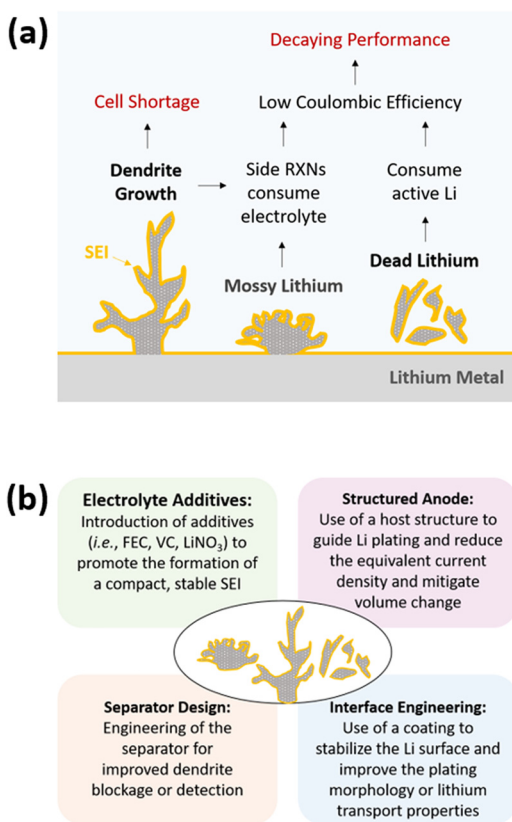


**FIG. 1.** (a) Proposed failure and degradation mechanisms for the Li metal anode. (b) Summary of four general approaches to improve Li metal anodes reported previously.

This Perspective details the use of alloy type surface modifications and coatings to (1) analyze the dendrite suppression mechanisms and (2) discuss insight and strategies for the interfacial stability of the Li metal anode. Figure 2 shows various thermodynamically and kinetically controlled approaches for both surface modifications and coatings on Li metal anodes with the increasing effective interfacial thickness. Hypotheses including mechanical suppression of Li dendrites, selective Li ion diffusion through the coating, and thermodynamic aspects of lithiophilic substrates are discussed below, along with the role of ionic conductivity and Li nucleation with interfacial coatings. Finally, a future outlook on thermodynamically controlled interfacial engineering is discussed.

The idea of using Li-rich alloys for Li dendrite suppression was suggested by Huggins in the 1980s.<sup>21,22</sup> Improved Li deposition morphology on Li-alloys was hypothesized to be the result of fast Li surface diffusion. Note that the term “Li-alloys” in the battery literature includes intermetallics or composites, while the term “alloys” usually refers only to solid solutions in physical metallurgy. A similar argument based on surface diffusion was proposed by Shi *et al.*<sup>23,24</sup> from studies of Li-Mg and Li-Zn alloys fabricated through physical vapor deposition [thermal evaporation; Fig. 2(d)]. More recently, studies from Archer’s group showed improved Li plating morphology and Coulombic efficiency using Li-In<sup>25</sup> and Li-Sn<sup>26</sup> coatings formed on

the lithium surface through the spontaneous reduction of In(TFSI)<sub>3</sub> and SnTFSI [TFSI = bis(trifluoromethylsulfonyl)imide] salt solutions, respectively [Fig. 2(e)]. Similar beneficial effects were also observed for Li-Si coating fabricated by sputtering Si on Li [Fig. 2(c)],<sup>27</sup> and Li-Al coating made by laminating an Al foil onto Li [Fig. 2(g)].<sup>28</sup>

Improvements in plated Li morphology are generally attributed to faster Li surface diffusion in the “alloyed” layer. Chemical diffusion coefficients of Li in the surface layers are obtained through the galvanostatic intermittent titration technique,<sup>29</sup> and the diffusion coefficient of Li in Li-rich alloy phases<sup>21,22,24</sup> is generally more than two orders of magnitude higher than Li self-diffusion in bulk Li.<sup>30</sup> Based on density functional theory (DFT) calculations, Archer *et al.* showed that Li ions exhibit fast surface transport on indium, which helps to explain the observed uniform Li deposition on the indium coating layer.<sup>25</sup>

Moreover, Li nucleation shows zero overpotential on metal substrates where Li has at least some solubility and is able to form an alloy, such as Au, Ag, and Mg.<sup>31</sup> This phenomenon can be explained from a nucleation point of view. Plating Li on top of a metal with negligible solid solubility would require heterogeneous nucleation, which means that the system has to overcome a positive nucleation barrier that results in an overpotential.<sup>32</sup> On the other hand, the room temperature solubility of Li in Au, Ag, and Mg enables the formation of a surface solid solution layer upon lithiation at the interface without the need for heterogeneous nucleation, thereby eliminating the overpotential associated with the nucleation process. This surface layer also alters the morphology of the deposited Li.<sup>33–35</sup> Furthermore, studies have shown that “dead Li” formation depends more on the nucleation process, rather than the subsequent growth.<sup>36–38</sup> Therefore, it can be inferred that a substrate with preferred nucleation can decrease the dead Li formation and improve the cycling Coulombic efficiency.

Another, and perhaps better, approach is to enable the nucleation of Li underneath the coating. Nazar *et al.* reported uniform Li plating below an ~10 μm composite layer consisting of a lithium-rich intermetallic (Li-In, Li-As, Li-Bi, and Li-Zn) and metal chloride species.<sup>39</sup> The proposed mechanism in this particular study focused on the role of the high Li-diffusivity in the intermetallic component of the coating, which is hypothesized to transport Li solely. It was further postulated that the presence of lithium chloride, a by-product of the reaction used to form the layer, serves to impart electronic resistivity to the composite layer to inhibit the reduction of lithium on the outer surface of the coating. Subsequent papers on Li-Ge coating from GeCl<sub>4</sub>-THF steam treatment<sup>40</sup> and Li-Sb coating from SbI<sub>3</sub> solution<sup>41</sup> reported similar phenomena. For these systems, it is argued that fast Li diffusion in Li-rich compounds plays a critical role in enabling lithium transport through the layer instead of on the surface.

When lithium plating occurs underneath a coating layer, the performance improvements are hypothesized to be associated with the mechanical suppression of dendrite growth and selective Li-ion transport.<sup>39</sup> Theoretical models have shown that a coating material under conformal compressive stress with a shear modulus that is higher than Li can cause preferential deposition of Li in concave regions (rather than at peaks), thereby reducing the surface roughness of the deposited Li.<sup>42,43</sup> Interestingly, these composite coatings are proposed to exhibit selective Li-ion transport across the coating while blocking the anions, thus preventing the occurrence of side reactions between Li and the electrolyte.<sup>39</sup> The fast Li transport properties of Li-rich alloys were also argued to provide a uniform Li flux across the

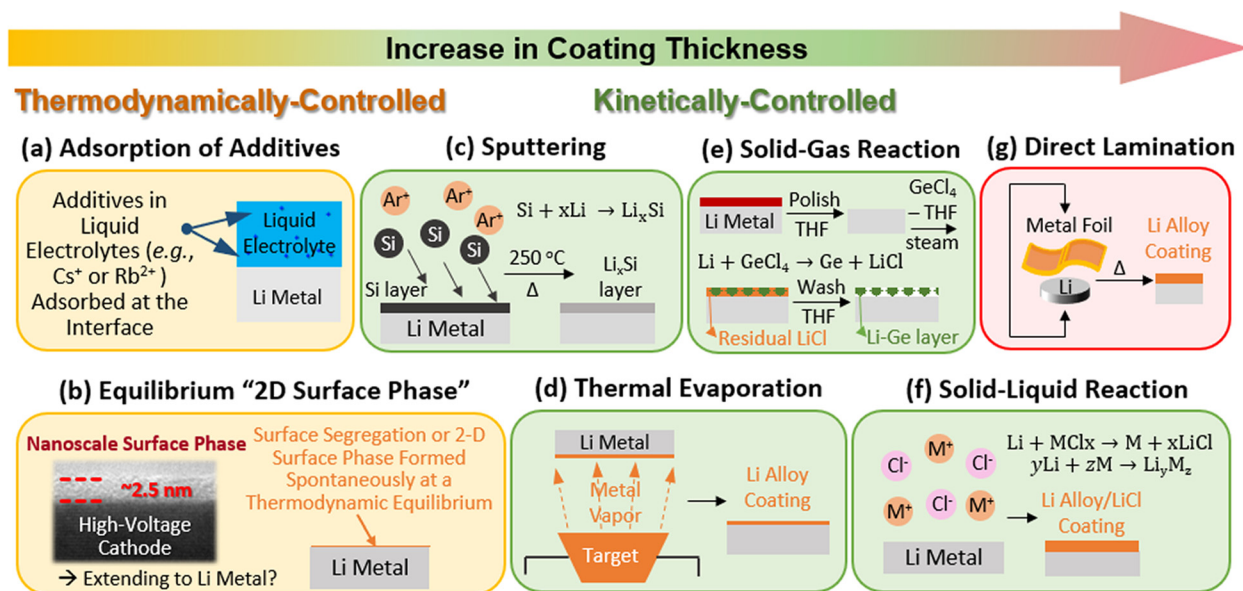


**FIG. 2.** Schematic illustration of various methods for surface modifications and coatings with the increasing effective interfacial thickness. (a) It should be noted that the adsorption of cations<sup>62</sup> (e.g., Cs<sup>+</sup> and Rb<sup>2+</sup>) from the additives in liquid electrolytes on the surface of liquid metals represents a case of thermodynamically controlled surface modification (albeit it is not the focus of this Perspective). (b) Likewise, we propose to utilize surface segregation (or spreading of a wetting or prewetting precursor film<sup>63</sup>) or equilibrium formation of 2D surface phases, which have been proven to be feasible and useful to improve the stability of cathode surfaces,<sup>89</sup> as a potentially new surface engineering method for lithium metal anodes (yet to be explored). More commonly adopted, various kinetically controlled surface coatings to improve lithium metal anodes include (c) Li<sub>x</sub>Si layer fabricated from sputtering and annealing.<sup>27</sup> (d) Alloy coatings formed by metal evaporation onto the Li metal surface.<sup>23,24</sup> (e) Li-Ge-based surface modification synthesized from spontaneous reaction between Li and GeCl<sub>4</sub>-THF vapor.<sup>40</sup> (f) Alloy-LiCl composite protection layer synthesized from reaction between Li and metal chloride solution.<sup>39</sup> (g) Finally, direct lamination of metal foils on lithium with controlled pressure and temperature represents another method to make even thick alloy type interfacial layers.<sup>28</sup> Panel (a) is adapted with permission from Ding *et al.*, *J. Am. Chem. Soc.* **135**, 4450 (2013). Copyright 2013 American Chemical Society. Panel (b) is reprinted with permission from J. Huang and J. Luo, *Phys. Chem. Chem. Phys.* **16**, 7786 (2014). Copyright 2014 PCCP Owner Societies. Panel (c) is adapted with permission from Tang *et al.* *Adv. Mater.* **30**, 1801745 (2018). Copyright 2018 Wiley-VCH. Panel (e) is adapted with permission from, Liao *et al.*, *Adv. Mater.* **30**, 1705711 (2018). Copyright 2018 Wiley-VCH.

layer, resulting in deposition underneath the coating.<sup>39</sup> Table I summarizes the Li-ion diffusion coefficients for various Li-rich intermetallic compounds. Using Li<sub>22</sub>Sn<sub>5</sub> as an example, room temperature Li diffusion coefficients were found to be in the range between  $1.9 \times 10^{-7}$  and  $5.9 \times 10^{-7}$  cm<sup>2</sup> s<sup>-1</sup> based on electrochemical measurements.<sup>44</sup> This is significantly higher than the diffusion coefficient of Li in bulk Li metal ( $7.65 \times 10^{-11}$  cm<sup>2</sup> s<sup>-1</sup>).<sup>30</sup>

Although many studies have reported improvements on plating morphology and cycling stability, Li-metal anodes are still far from commercialization. More studies are needed to understand cell failure mechanisms with these applied coatings. In the case of Li plating underneath the coating layer, the proposed working mechanisms (mechanical suppression and selective ion diffusion) assume that the coating can remain undamaged upon cycling. However, this assumption requires further experimental validation. Cell stacking pressure means that deformation can occur along with Li plating. Moreover, stripping can easily cause cracks to form on the coating. As shown in Fig. 3, dense, conformal, and micrometer-thick coatings consisting of Li salts or intermetallic compounds are brittle<sup>45</sup> and do not allow for the plastic deformation that results from the Li volume change on cycling. A similar argument has also been proposed for the LiPON protection layer on Li metal anodes. LiPON, which is commonly used as a solid-state electrolyte, produces an ion-conducting and relatively

brittle coating. The cycling stability of LiPON protected Li was enhanced at low plating/stripping capacity. Unfortunately, for high energy density cells, cracks were observed due to the substantial volume changes in the Li metal, and dendrites eventually formed.<sup>46,47</sup> For interfacial coatings that favor Li plating underneath, there likely exists a current density threshold for effective dendrite suppression. Providing a unified testing protocol or computation model to identify and predict areal capacity/current density limitations exceeds the scope of this Perspective. However, it is worth noting that studies are needed to identify this threshold and factors that determine it, with the goal of eventually increasing this threshold value.

Although the use of a lithiophilic substrate, such as Li-In<sup>25</sup> and Li-Sn<sup>31</sup> interfacial coatings, has been shown to alter the initial nucleation process, their beneficial effects on the subsequent growth and cycling are questionable. As shown in Fig. 3, after the nuclei cover a significant area on the substrate, the plated Li becomes the substrate for the incoming Li-ion, and the deposition morphology mainly depends on Li-ion mass transfer in the liquid electrolyte.<sup>48</sup> At high Li plating current densities, Li-ion diffusion in the electrolyte becomes the limiting process, and a concentration gradient builds up near the deposition surface. The resulting electric field causes fractal dendrites to grow.<sup>38</sup> Moreover, since the plated Li is in direct contact with the liquid electrolyte, side reactions between Li and the electrolyte

**TABLE I.** A summary of Li diffusivity in various Li-rich alloy type coatings. In the method column, the following abbreviations are used: nuclear magnetic resonance (NMR) and galvanostatic intermittent titration technique (GITT).

Material	Li diffusivity ( $\text{cm}^2 \text{s}^{-1}$ )	Temperature	Method	References
Li (self-diffusion)	$7.65 \times 10^{-11}$	25 °C	NMR	100
	$6.12 \times 10^{-11}$	25 °C	Thermodynamic Model	30
$\text{Li}_{13}\text{Sn}_5$	$5.01 \times 10^{-5} - 7.59 \times 10^{-4}$	415 °C	GITT	101
$\text{Li}_{22}\text{Sn}_5$	$1.9 \times 10^{-7} - 5.9 \times 10^{-7}$	25 °C	GITT	44
	$6.58 \times 10^{-5} - 1.91 \times 10^{-4}$	415 °C	GITT	101
$\text{Li}_{22}\text{Si}_5$	$5.13 \times 10^{-5} - 7.24 \times 10^{-5}$	415 °C	GITT	102
$\text{Li}_3\text{Sb}$	$2.0 \times 10^{-4} - 4.0 \times 10^{-4}$	360 °C	GITT	103
$\text{Li}_3\text{Bi}$	$1.0 \times 10^{-6} - 3.0 \times 10^{-6}$	25 °C	GITT	104
$\text{LiZn}$	$4.0 \times 10^{-7} - 4.0 \times 10^{-8}$	25 °C	GITT	24, 44
Li-In (47–62 at % Li)	$4.73 \times 10^{-7} - 3.98 \times 10^{-5}$	415 °C	GITT	105
$\text{Li}_x\text{Ag}$ ( $x = 4.7-5.0$ )	$0.12 \times 10^{-8} - 4.0 \times 10^{-8}$	25 °C	GITT	106
Li-Mg ( $\beta$ -phase)	$\approx 10^{-8}$	25 °C	GITT	23
	$\approx 10^{-11}$	25 °C	Neutron tomography	107
	$2.3 \times 10^{-11}$	25 °C	Sand's equation	108

continue to occur and consume the electrolyte. Therefore, while lithophilic substrates demonstrate improved morphology and growth of Li deposits initially, there is a limitation on the effectiveness of this approach once the surface of the coating is fully (or partially) covered by lithium.

To fully comprehend the mechanisms of coating and further improve it, the microstructure, ion conduction mechanisms, and Li nucleation behaviors all require further studies. Specifically, Li conduction through a micrometer-thick composite coating on Li metal consisting of a Li-rich intermetallic compound and Li salts, as shown in Fig. 2(f), is complex. In the case of a fully dense coating, the only ion pathway for the observed deposition of Li underneath the coating is through the intermetallic compound network. Since the Li-ion diffusion coefficient in the organic electrolyte is usually higher than the typical values in intermetallic compounds,<sup>22,49</sup> the rate-limiting step is

governed by the coating layer as Li ions diffuse from the liquid electrolyte, across the coating layer, and nucleate underneath. There will be a kinetic limitation for the maximum ion flux across the coating and, therefore, a current threshold above which it becomes favorable for Li to nucleate on the top of the coating. The inherent ionic diffusivity of the coating layer and the coating thickness are important parameters to tune this current threshold. Previous studies have also pointed out that the desolvation of Li ions from the solvent molecule determines the activation energies of Li-ion transport across the liquid/solid interface.<sup>50,51</sup> The solvation ability of the electrolyte solvent can be tuned with different Li salts. A recent study of Li-ion transport at the  $\text{LiNi}_{0.33}\text{Mn}_{0.33}\text{Co}_{0.33}\text{O}_2$ /electrolyte interface reported that Lithium bis(trifluoromethane)sulfonimide (LiTFSI)-based electrolyte can have an  $\sim 100$ -fold increase in exchange current density at the solid-liquid electrolyte interface in comparison to the  $\text{LiPF}_6$ -based electrolyte.<sup>52</sup> This behavior was attributed to the lower desolvation energy of  $\text{Li}^+$  with TFSI.

Moreover, composite films are almost never fully dense, e.g., the microstructures of the composite coatings like those shown in Fig. 2(f) that enable underneath Li plating. Thus, more careful characterization is required. Porosity may exist in such a composite coating layer due to salt dissolution and inherent defects; if the pores are connected above a percolation threshold, Li conduction can occur through the percolated electrolyte within the coating. Here, characterization via cryogenic electron microscopy (cryoEM) can potentially provide more detailed information on the coating microstructure without severe beam damage.<sup>53</sup> Evaluation of changes in the coating structure and in the location of Li nucleation with different current densities can be done using a variety of methods, including *in situ* x-ray tomography<sup>54</sup> and ex-situ cryo-focused ion beam-scanning electron microscopy (Cryo-FIB-SEM).<sup>55</sup> Direct imaging methods such as these can be helpful in understanding the coating degradation mechanism and to provide insights for the future design of protection coatings.

Figure 4 depicts several essential attributes of one ideal interfacial protection layer for the Li metal anode.<sup>3,6</sup> A coating that allows for

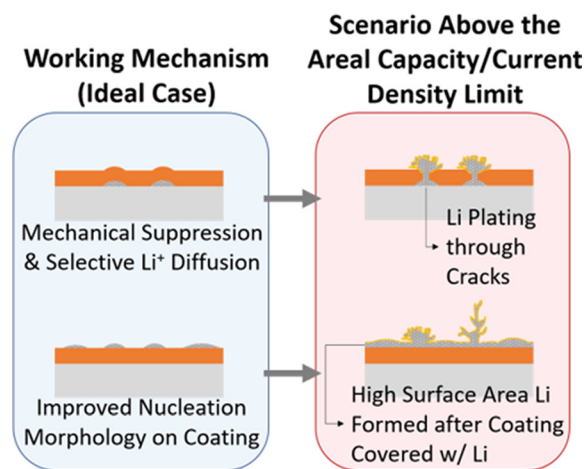


**FIG. 3.** Schematics of possible failure mechanisms of alloy type coatings after the areal capacity or current density limit is exceeded.

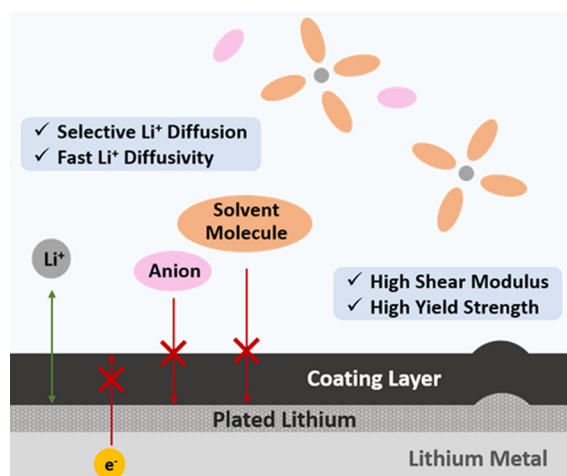


FIG. 4. Schematic illustration of ideal features of the interfacial protection layer on lithium metal.<sup>3,6</sup>

lithium deposition to take place underneath, as is likely achieved in the case shown in Fig. 2(f), is preferred for a dendrite-free anode. Unlike Li plating on top, the effectiveness of suppressing Li dendrites focuses less on the nucleation process and more on the effective transport and lithium flux across the coating layer. Having fast, selective lithium transport through the layer is a critical requirement. For example, previous studies already suggested that solid electrolyte type coatings can allow selective Li-ion diffusion, while no anion species can diffuse across the layer.<sup>50,51</sup> Li transport across the layer must be kinetically faster than the process of plating on top of the layer. Sluggish transport kinetics could result in the layer transport process becoming a rate-limiting step, leading to concentration gradients within the layer and added polarization. Additionally, having high electronic resistance in the layer is beneficial, as it provides a less favorable environment for lithium reduction on the surface of the coating layer, effectively reducing the kinetics for lithium plating on top of the layer and, thus, allowing Li transport through the films to better compete kinetically. In the case of the work of Nazar *et al.*,<sup>39</sup> the composite nature of the layer with a chlorine species fulfilled this need, but potentially reduced the Li transport rate due to the large “inactive” component to the film. In addition to selective and fast Li-ion diffusion, the coating layer should be thermodynamically stable with Li metal. Specifically, solid electrolyte coatings have good Li-ion conductivity, but many of them are not stable in contact with Li metal. One such example is  $\text{Li}_{1+x}\text{Al}_x\text{Ge}_{2-x}(\text{PO}_3)_3$  (LAGP), where  $\text{Ge}^{4+}$  can be reduced by Li metal.<sup>56</sup> More discussion about solid electrolyte coatings and their stability can be found elsewhere.<sup>57,58</sup>

It is also worth acknowledging that at higher currents, there exists a threshold where plating on top of the layer will be more kinetically favorable. Further studies are needed to design a layer where the threshold can be pushed further toward high power usage.

Despite its potential advantages, plating underneath a coating layer results in volume expansion and stress build-up from the plated lithium that must be accommodated. Therefore, the mechanical properties of the layer should also be considered as the layer material must be able to withstand the stress fluctuations generated by the plating

and stripping process. To better accommodate the volume expansion, one strategy is to combine inorganic coating materials with various polymers to form a composite coating with increased elasticity.<sup>59,60</sup> Alternatively, the interfacial coating can be combined with a 3D porous Li-host structure to alleviate the volume changes during Li plating and stripping.<sup>20</sup>

Finally, self-healing, where a coating can repair itself or rebuild during cycling, would be a highly desirable feature for any protective coating. Some of the self-healing functions may be achieved in thermodynamically controlled coatings that form spontaneously.

As described in the preceding sections, current research on interfacial engineering of the Li metal anode is generally based on kinetically controlled methods. Here, the thickness of the coating is controlled by the supply of the coating-forming material, e.g., via sputtering [Fig. 2(c)], vapor deposition [Fig. 2(d)], and reactions with vapor [Fig. 2(e)] or solution [Fig. 2(f)], or the thickness of the initial metal foil [Fig. 2(g)]. In other words, the thickness of the coating is not self-limiting. Another issue with any kinetically controlled coating method is the relatively high possibility of forming defects in the coating.

As the field moves forward, we may further exploit interfacial engineering based on thermodynamic approaches.<sup>61</sup> One example, albeit not the focus of this Perspective, is represented by the adsorption of cations such as  $\text{Cs}^+$  and  $\text{Rb}^{2+}$  from additives in the liquid electrolytes on the Li metal surface [Fig. 2(a)],<sup>62</sup> which will form adsorbates that serve as a “protective coating” on the lithium anode. Such adsorption can be viewed to form spontaneously at thermodynamic equilibrium. Therefore, it may rebuild (though it can be inhibited by SEI formation) upon Li plating and stripping to self-heal and provide uniform Li deposition. An in-depth discussion of this approach is beyond the scope of this Perspective, but can be found in other reviews of electrolyte additives.<sup>2,9</sup>

A good example of thermodynamically controlled interfacial engineering is to alloy (dope) Li with a surface-active or segregating metal element  $M$  to promote the surface segregation of  $M$  in a Li- $M$  system as a spontaneously formed protective “coating.” Equivalently in thermodynamics, segregation is the same as adsorption at a thermodynamic equilibrium; a surface phase can form via segregation/adsorption of a dopant (alloying element) or spreading of a prewetting precursor film.<sup>63</sup> In a broader context, Figure 5 shows that various 2D interfacial phases can form at thermodynamic equilibria.<sup>64–66</sup> These interfacial phases form spontaneously (which may lead to fewer defects in comparison with kinetically controlled coating processing) when chemical segregation couples with interfacial structural transitions (e.g., reconstruction) or disordering (e.g., formation of premelting like interfacial layers).<sup>64</sup> Such interfacial phases, which are 2D thermodynamically (that is, no degree of freedom in the third dimension perpendicular to the interface), have been named as complexions<sup>64</sup> to differentiate them from thin layers of bulk (3D) phases present at interfaces (with arbitrary or “kinetically controlled” thicknesses). In other words, a 2D interfacial phase (or complexion) should exhibit a thermodynamically determined or self-selecting thickness (independent of kinetic factors, once a thermodynamic equilibrium is achieved).<sup>64</sup> While it is successfully applied to improve the performance of various cathodes [Figs. 2(b) and 5(d)] and other anodes such as  $\text{TiO}_2$  [Fig. 5(c)], this Perspective for interfacial engineering has yet to be explored for Li metal anodes.

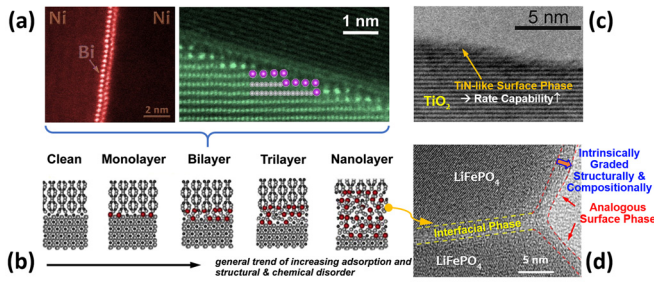


**FIG. 5.** Perspectives on thermodynamically controlled interfacial engineering. (a) Example of ordered bismuth adsorption at nickel general grain boundaries.<sup>65,66</sup> (b) Schematic illustration of a series of 2D interfacial phases at grain boundaries<sup>64</sup> and presumably also hetero-phase interfaces. (c) Surface nitridation of  $\text{TiO}_2$  Li-ion battery anode material to form  $\text{TiO}_x\text{N}_y$ -based (TiN-like) surface phases to increase the rate capability and surface electronic conductivity.<sup>90</sup> (d) Enhanced  $\text{Li}^+$  conductivity from utilizing analogous 2D interfacial phases at surfaces and grain boundaries in  $\text{LiFePO}_4$  cathode material.<sup>93</sup> Panel (a) is reprinted with permission from Luo *et al.*, *Science* **333**, 1730 (2011). Copyright 2011 American Association for the Advancement of Science. Panel (b) is reprinted with permission from Cantwell *et al.*, *Acta Mater.* **62**, 1 (2014). Copyright 2014 Elsevier. Panel (c) is reprinted with permission from M. Samiee and J. Luo, *J. Power Sources* **245**, 594 (2014). Copyright 2014 Elsevier. Panel (d) is reprinted with permission from Kayyar *et al.*, *Appl. Phys. Lett.* **95**, 221905 (2009). Copyright 2009 AIP Publishing.

Let us briefly explain the underlying physics of the formation of 2D interfacial phases in several steps, as follows. First, we consider that the  $\beta$  phase can perfectly wet an  $\alpha$ - $\gamma$  interface if

$$\gamma_{\alpha\beta} + \gamma_{\beta\gamma} < \gamma_{\alpha\gamma}^{(0)}, \quad (1)$$

where  $\gamma_{\alpha\beta}$ ,  $\gamma_{\beta\gamma}$ , and  $\gamma_{\alpha\gamma}^{(0)}$  are the interfacial energies of  $\alpha$ - $\beta$ ,  $\beta$ - $\gamma$ , and  $\alpha$ - $\gamma$  interfaces, respectively, and the superscript “(0)” in  $\gamma_{\alpha\gamma}^{(0)}$  denotes it is a hypothetical “clean” interface without the wetting or adsorption (while the equilibrium  $\gamma_{\alpha\gamma} \equiv \gamma_{\alpha\beta} + \gamma_{\beta\gamma}$  for the case of perfect wetting).<sup>63</sup> Second, if the  $\beta$  phase is not stable as a (3D) bulk phase, a  $\beta$ -like (2D) interfacial phase (of microscopic thickness  $h$ ) can still be stabilized at the  $\alpha$ - $\gamma$  interface thermodynamically by the reduction of interfacial energies ( $-\Delta\gamma$  defined below), if

$$-\Delta\gamma \equiv \gamma_{\alpha\gamma}^{(0)} - (\gamma_{\alpha\beta} + \gamma_{\beta\gamma}) < \Delta G_{\beta}^{(vol)} \cdot h, \quad (2)$$

where  $\Delta G_{\beta}^{(vol)}$  is the volumetric free energy penalty for forming the metastable  $\beta$  phase.<sup>67–69</sup> This phenomenon is called “prewetting” in physics, which refers to “wetting” occurring when the phase does, the wetting is not yet a stable bulk phase.<sup>63,70,71</sup> Third, in a phenomenological thermodynamic theory, the interfacial excess grand potential of this  $\beta$ -like interfacial phase can be written as<sup>67,68</sup>

$$\Phi^x = \gamma_{\alpha\gamma}^{(0)} + \Delta\gamma \cdot f(h) + \Delta G_{\beta}^{(vol)} \cdot h. \quad (3)$$

Here,  $f(h)$  is a dimensionless interfacial coefficient that describes the details of the thickness-dependent interfacial interactions, which should satisfy the boundary conditions:  $f(0) = 0$  and  $f(+\infty) = 1$ . Minimization of the interfacial excess grand potential in Eq. (3) defines the equilibrium interfacial configuration (with an “equilibrium” or thermodynamically determined thickness  $h_{\text{EQ}}$ ). In a continuum

approximation, the interfacial coefficient depends on the thickness exponentially if a short-range interaction dominates or quadratically if an unretarded London dispersion force dominates.<sup>67–69</sup> For an idealized “hard-sphere” liquid, an additional oscillatory structural (solvation) interaction<sup>72</sup> arises, producing an idealized series of discrete complexions,<sup>64</sup> i.e., clean, monolayer, bilayer, trilayer, nanolayer, and wetting layer complexions, as shown in Fig. 5(b). In other words, these six complexions correspond to  $h_{\text{EQ}} = 0, 1\sigma, 2\sigma, 3\sigma, x$  ( $\sim 1$  nm), and  $+\infty$ , respectively, where  $\sigma$  is the thickness of a monolayer of adsorbates.<sup>73</sup> This series of complexions have been discovered by Dillon *et al.*<sup>74</sup> at  $\text{Al}_2\text{O}_3$  grain boundaries with different dopants, but they can also exist in other types of interfaces. A more rigorous thermodynamic model can be found in Ref. 75, with further discussion in an overview article.<sup>64</sup> For Li-M systems, however, the interfacial coefficient  $f(h)$  should be more complex than the overly simplified “hard spheres” model due to strong Li-M bonding, and so we do not expect a simple series of Dillon-Harmer complexions to occur in a sequence. Here, reconstruction like those observed in the Ni-Bi,<sup>65,66</sup> Cu-Bi,<sup>76</sup> Al-Cu,<sup>77</sup> and Si-Au,<sup>73,78</sup> or transition metal-doped WC<sup>79</sup> is expected (with possibly even more complexity and diversity). Disordered interfacial phases (nanoscale amorphous-like intergranular films) similar to those observed in W-Ni,<sup>80,81</sup> Mo-Ni,<sup>82</sup> Ni-W,<sup>83</sup> Ni-S,<sup>84</sup> Cu-Zr,<sup>85</sup> and Cu-Zr-Hf<sup>86</sup> may also exist in certain Li-M systems. Noting that the above thermodynamic framework is applicable surfaces, grain boundaries, and other types of interfaces. The specific atomic configurations for 2D interfacial phases in Li-M systems, which should also depend on the specific metal M, have yet to be characterized experimentally.

Different from previously discussed kinetically controlled coatings where the thickness is determined by the amount of coating material supplied or the processing time [Figs. 2(c)–2(f)], a thermodynamically controlled 2D surface phase can form spontaneously with a self-limiting thickness at a thermodynamic equilibrium.<sup>61</sup> Previous studies have demonstrated that  $\text{Li}_3\text{PO}_4$ -based surface amorphous films (SAFs), which are a type of 2D surface phase with a self-selecting or “equilibrium” thickness on the order of one nanometer, can form and improve cycling stability and rate capability of various cathode materials, including  $\text{LiNi}_{0.5}\text{Mn}_{1.5}\text{O}_4$ ,  $\text{LiCoO}_2$ , and  $\text{Li}_{1.33}\text{Ni}_{0.3}\text{Mn}_{0.57}\text{O}_4$  [see one example in Fig. 2(b)].<sup>87–89</sup>  $\text{WO}_3$ -based surface phases have also been used to improve the discharge capacities of  $\text{Li}_{1.33}\text{Ni}_{0.3}\text{Mn}_{0.57}\text{O}_4$  by decreasing the surface Ni/Mn ratio and changing the surface valence state.<sup>88</sup> Surface nitridation has been used to form a  $\text{TiO}_x\text{N}_y$ -based (or TiN-like) surface phase [Fig. 5(c), i.e., a “surface precursor” to the bulk TiN phase] to increase the rate capability of the  $\text{TiO}_2$  anode by increasing the surface electronic conductivity (resembling the properties of the conductive TiN).<sup>90</sup> It should be noted that most of these 2D surface phases formed in facile mixing and annealing at elevated temperatures. For low-melting lithium, if an equilibrium surface phase can form near room temperature, it may also be able to rebuild during cycling and serve as a self-healing surface coating—an intriguing direction that needs to be explored in future studies.

In addition to interfacial engineering of the Li metal anode, this thermodynamic approach also leads to other potential opportunities. Such interfacial complexions can also exist at grain boundaries to provide potential benefits.<sup>91,92</sup> For example, analogous phosphate-based “amorphous” films of equilibrium thicknesses on the order of one nanometer can form at both surfaces and grain boundaries of sintered  $\text{LiFePO}_4$  cathode particles to provide fast  $\text{Li}^+$  conduction pathways

[Fig. 5(d)].<sup>93,94</sup> Specifically, for the Li metal anode, premelting-like grain boundaries, which are the interfacial precursor to the liquid phase formed below the bulk melting temperature,<sup>70</sup> may form near room temperature. If so, this could provide super-plasticity (via promoting grain boundary sliding and Coble creep at room temperature), which would be a very desirable property. This effect represents yet another Perspective that needs to be verified and realized in a future study. Yet another possibility is to use complexions to tailor the interfaces in (kinetically controlled) thick protective coatings, e.g., to improve the interfacial ionic conductivity of the composite coatings similar to that shown in Fig. 2(f).

Advanced characterization is needed to elucidate the mechanism of interfacial phases. Various transmission electron microscopy (TEM) techniques including aberration-corrected scanning transmission electron microscopy (AC-STEM), energy dispersive X-ray spectroscopy (EDS), and electron energy loss spectroscopy (EELS) can be used to study the atomic level structure,<sup>65,95</sup> elemental composition,<sup>66</sup> and oxidation state of the interfacial phases,<sup>73</sup> respectively. *In situ* TEM setups<sup>96,97</sup> have been recently developed, which enables the characterization of dynamic changes of the interfacial phases in a real working environment. Due to the high reactivity of Li metal, TEM characterization needs to be conducted at cryogenic temperature to prevent electron beam damage on Li metal.<sup>53,98,99</sup> Care must be taken to prevent air exposure during the sample transfer as Li can easily react with oxygen, nitrogen, and water vapor. Cryo-FIB-SEM can also be used to study the cross section microstructure and Li deposition morphology.<sup>55</sup> Electrochemical impedance spectroscopy (EIS) combined with equivalent circuit model fitting can also be used to quantify bulk and interfacial charge transport properties.<sup>50</sup>

In general, 2D interfacial phases or complexions, which have structures that are neither observed in nor necessarily stable as conventional 3D bulk phases, can potentially help to obtain exceptional properties that many bulk phases cannot achieve alone, including ionic conductivity, interfacial stability, and cyclability. Some of these ideas have already been demonstrated for various battery systems, as discussed in a recent review.<sup>61</sup> Specifically, the feasibility of using 2D interface phases spontaneously formed at thermodynamic equilibria to tailor the lithium metal anode offers potential new opportunities, which must be further explored.

## AUTHORS' CONTRIBUTIONS

Q.Y. and G.W. contributed equally to this work.

This work was supported as part of the Center for Synthetic Control Across Length-scales for Advancing Rechargeables (SCALAR), an Energy Frontier Research Center funded by the United States Department of Energy, Office of Science, Basic Energy Sciences under Award No. DESC0019381.

## DATA AVAILABILITY

Data sharing is not applicable to this Perspective article as no new data were created or analyzed in this study.

## REFERENCES

- <sup>1</sup>M. S. Whittingham, *Science* **192**, 1126 (1976).
- <sup>2</sup>X. B. Cheng, R. Zhang, C. Z. Zhao, and Q. Zhang, *Chem. Rev.* **117**, 10403 (2017).
- <sup>3</sup>H. Zhou, S. Yu, H. Liu, and P. Liu, *J. Power Sources* **450**, 227632 (2020).
- <sup>4</sup>D. Lin, Y. Liu, and Y. Cui, *Nat. Nanotechnol.* **12**, 194 (2017).
- <sup>5</sup>L. Ma, M. S. Kim, and L. A. Archer, *Chem. Mater.* **29**, 4181 (2017).
- <sup>6</sup>R. Xu, X. B. Cheng, C. Yan, X. Q. Zhang, Y. Xiao, C. Z. Zhao, J. Q. Huang, and Q. Zhang, *Matter* **1**, 317 (2019).
- <sup>7</sup>J. B. Goodenough and Y. Kim, *Chem. Mater.* **22**, 587 (2010).
- <sup>8</sup>K. Xu, *Chem. Rev.* **104**, 4303 (2004).
- <sup>9</sup>K. Xu, *Chem. Rev.* **114**, 11503 (2014).
- <sup>10</sup>R. L. Sacci, N. J. Dudney, K. L. More, L. R. Parent, I. Arslan, N. D. Browning, and R. R. Unocic, *Chem. Commun.* **50**, 2104 (2014).
- <sup>11</sup>X. Q. Zhang, X. B. Cheng, X. Chen, C. Yan, and Q. Zhang, *Adv. Funct. Mater.* **27**, 1605989 (2017).
- <sup>12</sup>D. Aurbach, K. Gamolsky, B. Markovsky, Y. Gofer, M. Schmidt, and U. Heider, *Electrochim. Acta* **47**, 1423 (2002).
- <sup>13</sup>Y. Liu, D. Lin, Z. Liang, J. Zhao, K. Yan, and Y. Cui, *Nat. Commun.* **7**, 10992 (2016).
- <sup>14</sup>D. Lin, Y. Liu, Z. Liang, H. W. Lee, J. Sun, H. Wang, K. Yan, J. Xie, and Y. Cui, *Nat. Nanotechnol.* **11**, 626 (2016).
- <sup>15</sup>H. Wu, D. Zhuo, D. Kong, and Y. Cui, *Nat. Commun.* **5**, 5193 (2014).
- <sup>16</sup>M. S. Gonzalez, Q. Yan, J. Holoubek, Z. Wu, H. Zhou, N. Patterson, V. Petrova, H. Liu, and P. Liu, *Adv. Mater.* **32**, 1906836 (2020).
- <sup>17</sup>S. Bai, X. Liu, K. Zhu, S. Wu, and H. Zhou, *Nat. Energy* **1**, 16094 (2016).
- <sup>18</sup>S. Bai, Y. Sun, J. Yi, Y. He, Y. Qiao, and H. Zhou, *Joule* **2**, 2117 (2018).
- <sup>19</sup>E. Cha, M. D. Patel, J. Park, J. Hwang, V. Prasad, K. Cho, and W. Choi, *Nat. Nanotechnol.* **13**, 337 (2018).
- <sup>20</sup>Y. Gao, Z. Yan, J. L. Gray, X. He, D. Wang, T. Chen, Q. Huang, Y. C. Li, H. Wang, S. H. Kim, T. E. Mallouk, and D. Wang, *Nat. Mater.* **18**, 384 (2019).
- <sup>21</sup>R. A. Huggins, *J. Power Sources* **22**, 341 (1988).
- <sup>22</sup>R. A. Huggins, *J. Power Sources* **26**, 109 (1989).
- <sup>23</sup>Z. Shi, M. Liu, D. Naik, and J. L. Gole, *J. Power Sources* **92**, 70 (2001).
- <sup>24</sup>Z. Shi, M. Liu, and J. L. Gole, *Electrochem. Solid State Lett.* **3**, 312 (1999).
- <sup>25</sup>S. Choudhury, Z. Tu, S. Stalin, D. Vu, K. Fawole, D. Gunceler, R. Sundararaman, and L. A. Archer, *Angew. Chem.* **129**, 13250 (2017).
- <sup>26</sup>Z. Tu, S. Choudhury, M. J. Zachman, S. Wei, K. Zhang, L. F. Kourkoutis, and L. A. Archer, *Nat. Energy* **3**, 310 (2018).
- <sup>27</sup>W. Tang, X. Yin, S. Kang, Z. Chen, B. Tian, S. L. Teo, X. Wang, X. Chi, K. P. Loh, H. W. Lee, and G. W. Zheng, *Adv. Mater.* **30**, 1801745 (2018).
- <sup>28</sup>H. Kim, J. T. Lee, D. C. Lee, M. Oschatz, W. Il Cho, S. Kaskel, and G. Yushin, *Electrochem. Commun.* **36**, 38 (2013).
- <sup>29</sup>W. Weppner, *J. Electrochem. Soc.* **124**, 1569 (1977).
- <sup>30</sup>E. Dologlou, *Glas. Phys. Chem.* **36**, 570 (2010).
- <sup>31</sup>K. Yan, Z. Lu, H. W. Lee, F. Xiong, P. C. Hsu, Y. Li, J. Zhao, S. Chu, and Y. Cui, *Nat. Energy* **1**, 16010 (2016).
- <sup>32</sup>R. W. Balluffi, S. M. Allen, and W. C. Carter, *Kinetics of Materials* (John Wiley & Sons, 2005).
- <sup>33</sup>D. R. Ely and R. E. García, *J. Electrochem. Soc.* **160**, A662 (2013).
- <sup>34</sup>A. Pei, G. Zheng, F. Shi, Y. Li, and Y. Cui, *Nano Lett.* **17**, 1132 (2017).
- <sup>35</sup>K. S. Nagy, S. Kazemiabnavi, K. Thornton, and D. J. Siegel, *ACS Appl. Mater. Interfaces* **11**, 7954 (2019).
- <sup>36</sup>A. J. Sanchez, E. Kazyak, Y. Chen, K. H. Chen, E. R. Pattison, and N. P. Dasgupta, *ACS Energy Lett.* **5**, 994 (2020).
- <sup>37</sup>K. H. Chen, K. N. Wood, E. Kazyak, W. S. Lepage, A. L. Davis, A. J. Sanchez, and N. P. Dasgupta, *J. Mater. Chem. A* **5**, 11671 (2017).
- <sup>38</sup>K. N. Wood, M. Noked, and N. P. Dasgupta, *ACS Energy Lett.* **2**, 664 (2017).
- <sup>39</sup>X. Liang, Q. Pang, I. R. Kochetkov, M. S. Sempere, H. Huang, X. Sun, and L. F. Nazar, *Nat. Energy* **2**, 17119 (2017).
- <sup>40</sup>K. Liao, S. Wu, X. Mu, Q. Lu, M. Han, P. He, Z. Shao, and H. Zhou, *Adv. Mater.* **30**, 1705711 (2018).
- <sup>41</sup>T. Chen, W. Kong, P. Zhao, H. Lin, Y. Hu, R. Chen, W. Yan, and Z. Jin, *Chem. Mater.* **31**, 7565 (2019).
- <sup>42</sup>C. Monroe and J. Newman, *J. Electrochem. Soc.* **151**, A880 (2004).
- <sup>43</sup>C. Monroe and J. Newman, *J. Electrochem. Soc.* **152**, A396 (2005).
- <sup>44</sup>A. Anani and R. A. Huggins, **134**, 3098 (1987).
- <sup>45</sup>A. M. Russell, *Adv. Eng. Mater.* **5**, 629 (2003).
- <sup>46</sup>W. Liu, R. Guo, B. Zhan, B. Shi, Y. Li, H. Pei, Y. Wang, W. Shi, Z. Fu, and J. Xie, *ACS Appl. Energy Mater.* **1**, 1674 (2018).

- <sup>47</sup>A. C. Kozen, C. F. Lin, O. Zhao, S. B. Lee, G. W. Rubloff, and M. Noked, *Chem. Mater.* **29**, 6298 (2017).
- <sup>48</sup>J. Xiao, *Science* **366**, 426 (2019).
- <sup>49</sup>M. T. Ong, O. Vernal, E. W. Draeger, A. C. T. Van Duin, V. Lordi, and J. E. Pask, *J. Phys. Chem. B* **119**, 1535 (2015).
- <sup>50</sup>M. R. Busche, T. Drossel, T. Leichtweiss, D. A. Weber, M. Falk, M. Schneider, M. L. Reich, H. Sommer, P. Adelhelm, and J. Janek, *Nat. Chem.* **8**, 426 (2016).
- <sup>51</sup>Y. Yamada, F. Sagane, Y. Iriyama, T. Abe, and Z. Ogumi, *J. Phys. Chem. C* **113**, 14528 (2009).
- <sup>52</sup>B. Wen, Z. Deng, P. C. Tsai, Z. W. Lebens-Higgins, L. F. J. Piper, S. P. Ong, and Y. M. Chiang, *Nat. Energy* **5**, 578 (2020).
- <sup>53</sup>Y. Li, Y. Li, A. Pei, K. Yan, Y. Sun, C. L. Wu, L. M. Joubert, R. Chin, A. L. Koh, Y. Yu, J. Perrino, B. Butz, S. Chu, and Y. Cui, *Science* **358**, 506 (2017).
- <sup>54</sup>K. J. Harry, D. T. Hallinan, D. Y. Parkinson, A. A. MacDowell, and N. P. Balsara, *Nat. Mater.* **13**, 69 (2014).
- <sup>55</sup>J. Z. Lee, T. A. Wynn, M. A. Schroeder, J. Alvarado, X. Wang, K. Xu, and Y. S. Meng, *ACS Energy Lett.* **4**, 489 (2019).
- <sup>56</sup>Y. Zhu, X. He, and Y. Mo, *ACS Appl. Mater. Interfaces* **7**, 23685 (2015).
- <sup>57</sup>A. Banerjee, X. Wang, C. Fang, E. A. Wu, and Y. S. Meng, *Chem. Rev.* **120**, 6878 (2020).
- <sup>58</sup>Y. Xiao, Y. Wang, S. H. Bo, J. C. Kim, L. J. Miara, and G. Ceder, *Nat. Rev. Mater.* **5**, 105 (2020).
- <sup>59</sup>H. Zhang, C. Li, M. Piszcz, E. Coya, T. Rojo, L. M. Rodriguez-Martinez, M. Armand, and Z. Zhou, *Chem. Soc. Rev.* **46**, 797 (2017).
- <sup>60</sup>Z. Jiang, L. Jin, Z. Han, W. Hu, Z. Zeng, Y. Sun, and J. Xie, *Angew. Chem., Int. Ed.* **58**, 11374 (2019).
- <sup>61</sup>J. Luo, *Energy Storage Mater.* **21**, 50 (2019).
- <sup>62</sup>F. Ding, W. Xu, G. L. Graff, J. Zhang, M. L. Sushko, X. Chen, Y. Shao, M. H. Engelhard, Z. Nie, J. Xiao, X. Liu, P. V. Sushko, J. Liu, and J. G. Zhang, *J. Am. Chem. Soc.* **135**, 4450 (2013).
- <sup>63</sup>P. G. De Gennes, *Rev. Mod. Phys.* **57**, 827 (1985).
- <sup>64</sup>P. R. Cantwell, M. Tang, S. J. Dillon, J. Luo, G. S. Rohrer, and M. P. Harmer, *Acta Mater.* **62**, 1 (2014).
- <sup>65</sup>J. Luo, H. Cheng, K. M. Asl, C. J. Kiely, and M. P. Harmer, *Science* **333**, 1730 (2011).
- <sup>66</sup>Z. Yu, P. R. Cantwell, Q. Gao, D. Yin, Y. Zhang, N. Zhou, G. S. Rohrer, M. Widom, J. Luo, and M. P. Harmer, *Science* **358**, 97 (2017).
- <sup>67</sup>J. Luo, *Crit. Rev. Solid State Mater. Sci.* **32**, 67 (2007).
- <sup>68</sup>J. Luo and Y.-M. Chiang, *Annu. Rev. Mater. Res.* **38**, 227 (2008).
- <sup>69</sup>J. Luo, *J. Am. Ceram. Soc.* **95**, 2358 (2012).
- <sup>70</sup>J. W. Cahn, *J. Chem. Phys.* **66**, 3667 (1977).
- <sup>71</sup>D. Bonn, J. Eggers, J. Indekeu, and J. Meunier, *Rev. Mod. Phys.* **81**, 739 (2009).
- <sup>72</sup>J. N. Israelachvili, *Intermolecular and Surface Forces* (Academic Press, 2011).
- <sup>73</sup>S. Ma, P. R. Cantwell, T. J. Pennycook, N. Zhou, M. P. Oxley, D. N. Leonard, S. J. Pennycook, J. Luo, and M. P. Harmer, *Acta Mater.* **61**, 1691 (2013).
- <sup>74</sup>S. J. Dillon, M. Tang, W. C. Carter, and M. P. Harmer, *Acta Mater.* **55**, 6208 (2007).
- <sup>75</sup>J. Luo, *Appl. Phys. Lett.* **95**, 113115 (2009).
- <sup>76</sup>A. Kundu, K. M. Asl, J. Luo, and M. P. Harmer, *Scr. Mater.* **68**, 146 (2013).
- <sup>77</sup>P. Parajuli, D. Romeu, V. Hounkpati, R. Mendoza-Cruz, J. Chen, M. J. Yacamán, J. Flowers, and A. Ponce, *Acta Mater.* **181**, 216 (2019).
- <sup>78</sup>C. Hu and J. Luo, *Scr. Mater.* **158**, 11 (2019).
- <sup>79</sup>Z. Luo, C. Hu, L. Xie, H. Nie, C. Xiang, X. Gu, J. He, W. Zhang, Z. Yu, and J. Luo, *Mater. Horiz.* **7**, 173 (2020).
- <sup>80</sup>V. K. Gupta, D. H. Yoon, H. M. Meyer, and J. Luo, *Acta Mater.* **55**, 3131 (2007).
- <sup>81</sup>J. Luo, V. K. Gupta, D. H. Yoon, and H. M. Meyer, *Appl. Phys. Lett.* **87**, 231902 (2005).
- <sup>82</sup>X. Shi and J. Luo, *Phys. Rev. Lett.* **105**, 1 (2010).
- <sup>83</sup>J. D. Schuler, O. K. Donaldson, and T. J. Rupert, *Scr. Mater.* **154**, 49 (2018).
- <sup>84</sup>T. Hu, S. Yang, N. Zhou, Y. Zhang, and J. Luo, *Nat. Commun.* **9**, 2764 (2018).
- <sup>85</sup>A. Khalajhedayati, Z. Pan, and T. J. Rupert, *Nat. Commun.* **7**, 10802 (2016).
- <sup>86</sup>C. M. Grigorian and T. J. Rupert, *Acta Mater.* **179**, 172 (2019).
- <sup>87</sup>H. Liu, J. Huang, D. Qian, S. Hy, C. Fang, J. Luo, and Y. S. Meng, *J. Electrochem. Soc.* **163**, A971 (2016).
- <sup>88</sup>J. Huang, H. Liu, T. Hu, Y. S. Meng, and J. Luo, *J. Power Sources* **375**, 21 (2018).
- <sup>89</sup>J. Huang and J. Luo, *Phys. Chem. Chem. Phys.* **16**, 7786 (2014).
- <sup>90</sup>M. Samiee and J. Luo, *J. Power Sources* **245**, 594 (2014).
- <sup>91</sup>D. H. S. Tan, A. Banerjee, Z. Chen, and Y. S. Meng, *Nat. Nanotechnol.* **15**, 170 (2020).
- <sup>92</sup>J. Luo, *J. Mater.* **1**, 22 (2015).
- <sup>93</sup>A. Kayyar, H. Qian, and J. Luo, *Appl. Phys. Lett.* **95**, 221905 (2009).
- <sup>94</sup>B. Kang and G. Ceder, *Nature* **458**, 190 (2009).
- <sup>95</sup>T. Meiners, T. Frolov, R. E. Rudd, G. Dehm, and C. H. Liebscher, *Nature* **579**, 375 (2020).
- <sup>96</sup>X. H. Liu, L. Zhong, L. Q. Zhang, A. Kushima, S. X. Mao, J. Li, Z. Z. Ye, J. P. Sullivan, and J. Y. Huang, *Appl. Phys. Lett.* **98**, 183107 (2011).
- <sup>97</sup>R. R. Unocic, X. G. Sun, R. L. Sacci, L. A. Adamczyk, D. H. Alsem, S. Dai, N. J. Dudney, and K. L. More, *Microsc. Microanal.* **20**, 1029 (2014).
- <sup>98</sup>X. Wang, M. Zhang, J. Alvarado, S. Wang, M. Sina, B. Lu, J. Bouwer, W. Xu, J. Xiao, J.-G. Zhang, J. Liu, and Y. S. Meng, *Nano Lett.* **17**, 7606 (2017).
- <sup>99</sup>M. J. Zachman, Z. Tu, S. Choudhury, L. A. Archer, and L. F. Kourkoutis, *Nature* **560**, 345 (2018).
- <sup>100</sup>R. Messer and F. Noack, *Appl. Phys.* **6**, 79 (1975).
- <sup>101</sup>C. J. Wen and R. A. Huggins, *J. Solid State Chem.* **35**, 376 (1980).
- <sup>102</sup>C. J. Wen and R. A. Huggins, *J. Solid State Chem.* **37**, 271 (1981).
- <sup>103</sup>W. Weppner and R. A. Huggins, *J. Solid State Chem.* **22**, 297 (1977).
- <sup>104</sup>M. Hiratani, K. Miyauchi, and T. Kudo, *Solid State Ionics* **28-30**, 1406 (1988).
- <sup>105</sup>C. J. Wen and R. A. Huggins, *Mater. Res. Bull.* **15**, 1225 (1980).
- <sup>106</sup>S. Jin, Y. Ye, Y. Niu, Y. Xu, H. Jin, J. Wang, Z. Sun, A. Cao, X. Wu, Y. Luo, H. Ji, and L.-J. Wan, *J. Am. Chem. Soc.* **142**, 8818 (2020).
- <sup>107</sup>Y. Zhang, K. S. R. Chandran, M. Jagannathan, H. Z. Bilheux, and J. C. Bilheux, *J. Electrochem. Soc.* **164**, A28 (2017).
- <sup>108</sup>T. Krauskopf, B. Mogwitz, C. Rosenbach, W. G. Zeier, and J. Janek, *Adv. Energy Mater.* **9**, 1902568 (2019).